

Optical readout of a superconducting qubit using a piezo-optomechanical transducer

Received: 19 January 2024

Accepted: 22 November 2024

Published online: 11 February 2025

T. C. van Thiel¹, M. J. Weaver¹, F. Berto¹, P. Duivestein¹, M. Lemang¹, K. L. Schuurman¹, M. Žemlička¹, F. Hijazi¹, A. C. Bernasconi¹, C. Ferrer¹, E. Cataldo¹, E. Lachman², M. Field¹, Y. Mohan², F. K. de Vries³, C. C. Bultink³, J. C. van Oven³, J. Y. Mutus², R. Stockill¹ & S. Gröblacher¹

 Check for updates

Superconducting quantum processors have made important progress in size and computing potential. However, the practical cryogenic limitations of operating large numbers of superconducting qubits are becoming a bottleneck for further scaling. Due to the low thermal conductivity and the dense optical multiplexing capacity of telecommunications fibre, converting qubit signal processing to the optical domain using microwave-to-optics transduction would substantially relax the strain on cryogenic space and thermal budgets. Here we demonstrate optical readout of a superconducting transmon qubit through an optical fibre connected via a coaxial cable to a fully integrated piezo-optomechanical transducer. Using a demolition readout technique, we achieve a single-shot readout fidelity of 81%. Our results illustrate the benefits of piezo-optomechanical transduction for low-dissipation operation of large quantum processors.

Quantum computers are rapidly evolving from experimental settings towards commercially developed systems with ever-increasing numbers of qubits¹. Several important milestones have recently been achieved, including the first computations of problems that are practically infeasible to solve with even the largest classical computers^{2,3}. Nevertheless, solving tasks that are not merely proof-of-principle in character and could be of commercial interest, in particular with fault-tolerant operation, are still far beyond the reach of even the most advanced quantum processing units (QPUs)⁴. Superconducting processors, one of the leading architectures for QPUs, currently operate using a few hundred qubits, with roadmaps for scaling up to thousands^{5–8}. Scaling QPUs to these comparably small sizes will already require substantial improvements in cryogenic input–output technologies and necessitate dilution refrigerators that are many times larger than current systems⁹. With existing technology, much of the capacity in physical space and cooling power will be consumed by the amplifiers, circulators and coaxial cables required for controlling and reading out qubits. Reaching the millions of qubits anticipated to be required for fault-tolerant quantum computing applications¹⁰ therefore remains an elusive goal without notable technological leaps.

Mitigating these limitations by converting microwave signals to the optical domain is a promising approach to tackle this challenge and has attracted much interest^{11–16}.

Transducing qubit-state information to the optical domain allows a reduced passive heat load of the readout chain by up to three orders of magnitude¹⁷, as the thermal conductivity of optical fibres is negligible at cryogenic temperatures^{18,19}. Optical frequency readout can furthermore relax space constraints in the cryostat by eliminating or reducing the need for cryogenic amplification and add channel capacity through the use of dense optical multiplexing²⁰. Recent proof-of-principle experimental demonstrations of optical readout have used microwave-to-optics converters with three-dimensional optical²¹ or microwave²² cavities. However, three-dimensional transducer architectures for thousands of qubits exceed the spatial capacity of dilution refrigerators. Scalable optical readout of a superconducting qubit with large bandwidth, high repetition rate and a modular fibre-based approach has yet to be demonstrated.

Here, we demonstrate a fully integrated optical readout system that upconverts the readout tone from a transmon qubit, enabling faithful measurement of the qubit state. We verify the operation of

¹Qphox B.V., Delft, the Netherlands. ²Rigetti Computing Inc., Berkeley, CA, USA. ³Qblox B.V., Delft, the Netherlands.  e-mail: rob@qphox.eu; simon@qphox.eu

our optical readout system by measuring Rabi oscillations between the qubit ground and excited state, as well as by performing Ramsey interferometry. Our device is completely independent from the qubit itself and has a modular coaxial connection to the qubit chip. It consists of a microwave-to-optics transducer formed by an optomechanical nanobeam cavity coupled to a piezo-electric transducer, described in ref. 23. The fully integrated device, requiring a footprint of less than 0.15 mm^2 , allows direct scaling of the transducer from an individual proof-of-concept device to multiple channels, in principle being able to read out over a thousand qubits in parallel with only a few optical fibres.

We use a fixed-frequency transmon qubit hosted on a quantum integrated circuit test device²⁴ (qubit frequency $\omega_q/2\pi = 4.07 \text{ GHz}$), which is operated using microwave readout and control pulses, and dispersively coupled to a co-planar waveguide resonator (readout resonator frequency $\omega_r/2\pi = 5.1944 \text{ GHz}$). The output port of the single transmission line used to drive and read out the qubit is coupled to the microwave transmission line of a transducer chip via coaxial cables. A scanning electron microscope image of a representative transducer device is shown in Fig. 1a. The transducer and qubit chips are physically separated by around 40 cm, and the latter is magnetically shielded through multiple cryoperm casings, which also reduce the probability of stray light reaching the superconducting qubit. An illustration of the experimental configuration is shown in Fig. 1b. Microwave readout signals are upconverted by a piezo-optomechanical transducer operated with an optical pump tone red-detuned from the optical resonance ($\lambda_o = 1,564.891 \text{ nm}$, $\omega_o/2\pi = 191.57 \text{ THz}$) by the mechanical resonance frequency $\omega_m/2\pi = 5.1944 \text{ GHz}$. The optical pump tone is transmitted into the cryostat, where the light is sent towards the transducer via an edge coupler (40% coupling efficiency). The total detection efficiency of the reflected optical signal is 17% (see Supplementary Section I for further details). As discussed in previous work²³, the transducer incorporates a field-tunable microwave resonator to (1) resonantly enhance the electromechanical interaction with a LiNbO₃ piezo-electric block and (2) facilitate efficient coupling to a 50Ω transmission line.

Figure 1c shows the bidirectional microwave-to-optics conversion spectrum for different detunings of the transducer microwave resonator, under application of a continuous $3.1 \mu\text{W}$ red-detuned optical pump tone. The conversion efficiency is extracted using a four-port vector network analyser as described in ref. 25. Electrical signals incident on the transducer microwave port are upconverted to telecom light via first the piezo-electric and subsequently the optomechanical interaction. This process modulates the microwave signal onto the optical pump, which is reflected from the optical port of the transducer. The resulting optical signal is demodulated outside of the cryostat using heterodyne detection. From the conversion spectrum, we extract a peak efficiency of -24.8 dB (0.33%) at 5.1978 GHz with $3.1 \mu\text{W}$ of optical power, which is relatively insensitive to the detuning of the microwave resonator over a range of tens of megahertz, as shown in the inset of Fig. 1c. Figure 1d shows the efficiency as a function of the microwave drive frequency, exhibiting a -3 dB transduction bandwidth of 4.7 MHz , which is sufficiently large to facilitate state-of-the-art qubit readout at megahertz repetition rates^{2,26}. The dip in the spectrum corresponds to the qubit readout resonator frequency, which is shifted by 3.5 MHz from the peak, leading to a slightly reduced efficiency of -29.3 dB (0.12%). Due to the parametric nature of the optomechanical coupling rate²⁷, the transduction efficiency can be boosted by increasing the optical cavity photon number¹¹, that is, increasing the optical pump power, which is shown in Fig. 1e. We observe a linear increase of efficiency for the pump powers considered, consistent with the expected small optomechanical cooperativity at these powers and the large electromechanical cooperativity enabled by the piezo-electric interaction²⁸. At the largest optical power of $31 \mu\text{W}$, we extract efficiency values of 4% and 2% at the peak and qubit readout resonator frequencies, respectively. For the latter, this gives a value of $\sim 3 \times 10^{-3}$ for the overall quantum efficiency of the detection chain.

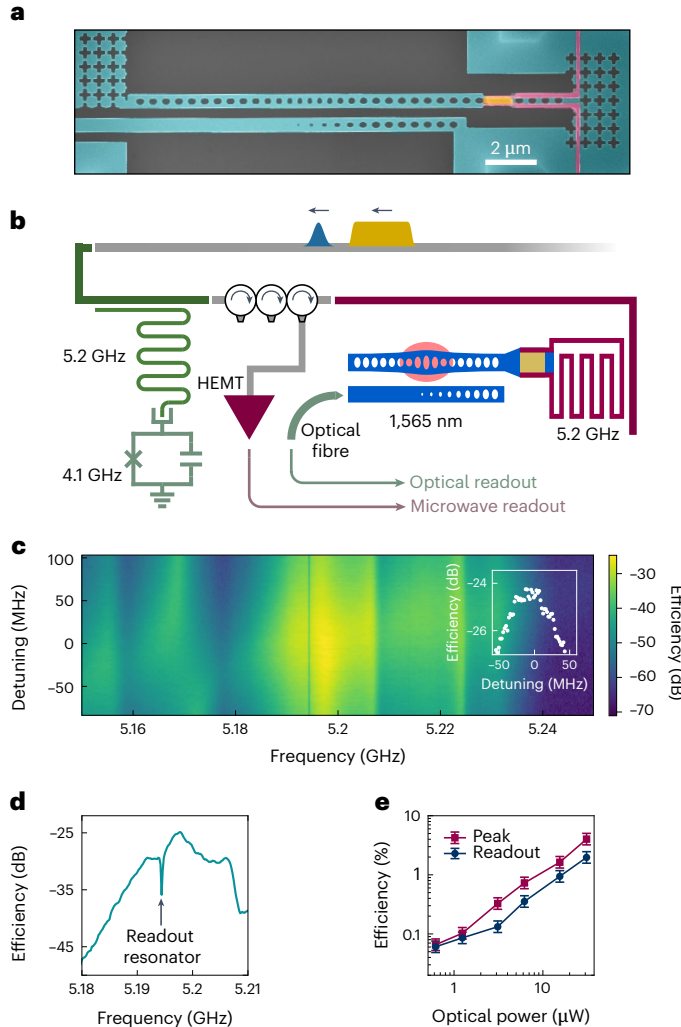


Fig. 1 | Transducer performance. **a**, A scanning electron microscope image of the piezo-optomechanical transducer comprising a piezo-electric block embedded in a superconducting resonator and an optomechanical photonic crystal cavity. **b**, An illustration of the experimental configuration for qubit readout using a piezo-optomechanical microwave-to-optics transducer. Microwave readout (yellow) and control (blue) pulses used to operate a fixed-frequency qubit are sent via coaxial cable into the transmission line of the transducer where the resulting qubit readout signal is upconverted to the optical domain. **c**, Continuous-tone bidirectional transduction efficiency under application of $3.1 \mu\text{W}$ optical pump power as a function of signal frequency and of microwave resonator detuning from the peak transduction frequency, with the inset showing a vertical linecut crossing the point of optimum efficiency. **d**, A horizontal linecut that shows a dip at 5.1944 GHz corresponding to the readout resonator of the qubit. **e**, The efficiency as a function of optical pump power, with the purple and blue lines representing the peak conversion efficiency and the efficiency at the qubit readout resonator frequency, respectively. The error bars represent the systematic errors.

To assess the potential of this device for optical qubit readout, we consider the contribution of optical heterodyne shot noise, which adds half a quantum of noise at the end of the optical detection chain. In our current configuration, referred back to the transducer microwave port, this yields an input-referred added noise of approximately 2×10^3 photons. This noise level impedes high-fidelity quantum non-demolition readout. However, it has been demonstrated that demolition readout can be used with high fidelity in transmon qubits^{29–31}. This approach exploits the occupation of higher level transmon states at large readout powers, which causes a qubit-state dependence of the power at which the readout resonator enters the bare regime³⁰. At such high

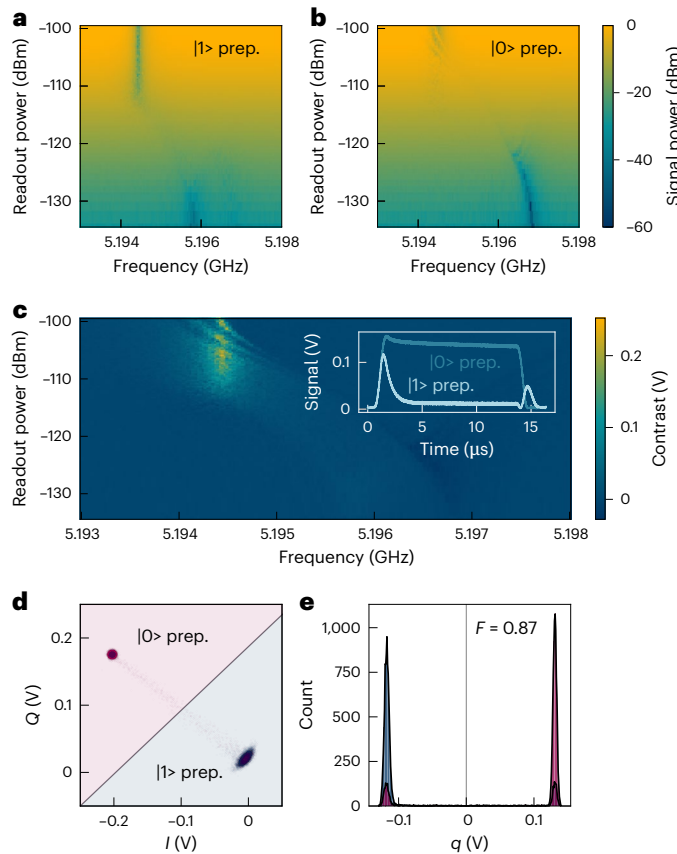


Fig. 2 | Microwave qubit readout. **a,b**, The readout signal magnitude for different readout frequencies and readout powers at the resonator with the $|1\rangle$ (**a**) and the $|0\rangle$ (**b**) state prepared (prep.). **c**, The signal voltage difference obtained by subtracting **b** from **a**. The inset shows averaged oscilloscope traces of the measured readout pulses, which have a duration of 14 μs and an integration window of 13.2 μs indicated by the vertical dashed lines to optimize the measured signal voltage difference between the two states. The largest difference is achieved at a readout power of -105.8 dBm at the bare resonator frequency 5.1944 GHz. **d,e**, The statistical characterization of 10,000 single-shot readout measurements in phase space (**d**) and binned by the distance q between each point to a linear decision boundary (**e**), with a readout fidelity $F = 0.87$.

readout powers, the signal is large enough to overcome typical amplifier noise at 4 K, enabling single-shot qubit readout without the use of a quantum-limited amplifier²⁹.

To define a benchmark for optical readout with a transducer, we proceed by characterizing the high-power readout fidelity with microwave signals only, using a 4 K high-electron-mobility transistor (HEMT) amplifier as the first amplifier in the microwave signal-processing chain. The microwave input readout signal is generated by upconverting signals from a commercially available base-band Qblox Qubit Readout Module to the radio frequency (RF) band with an I-Q mixer and delivered to the qubit transmission line³². The returned readout signal is interpreted through subsequent downconversion using an I-Q mixer, digitization and digital demodulation. Figure 2a,b shows the recorded microwave signal magnitude as a function of the frequency and amplitude of 14- μs -long readout pulses with the $|1\rangle$ and $|0\rangle$ qubit states prepared, respectively. Optimal signal voltage difference is achieved at the bare readout resonator frequency at a cavity drive power of -105.8 dBm (Fig. 2c). This readout power corresponds to a field amplitude in the readout resonator of $\sqrt{n_{\text{cav}}} \approx 90$ photons^{1/2}. The inset of Fig. 2c shows averaged oscilloscope traces of the detected readout signals at the point of optimal signal voltage difference. To obtain maximum difference between the two states, we choose a 13.2 μs

integration window, as indicated by the dashed vertical lines. Figure 2d shows the statistics of 10,000 single-shot readout measurements in phase space. We optimize a linear decision boundary to determine the experimental readout fidelity defined as $F = 1 - [p(1|0) + p(0|1)]/2$, which includes both state preparation and readout fidelity and serves as a lower bound for the readout fidelity (Fig. 2e). We extract a fidelity of $F = 87\%$, corresponding to an error rate of 6.5%, which we attribute to uncontrolled switching events. Such events can occur due to suboptimal thermalization of the qubit chip, thermally out-of-equilibrium quasiparticles^{33–35} or qubit energy relaxation during the readout pulse. From the number of photons in the readout pulse $\sim 1.1 \times 10^5$ and the signal-to-noise ratio (SNR) ~ 78 , given by the ratio of the separation and the standard deviation of the statistical distributions, we identify a microwave added noise level of -17 photons, which can largely be attributed to HEMT noise (-7 photons) in combination with 3 dB of loss introduced by the side-coupled qubit readout resonator.

Having optimized the high-power readout pulse and having set a benchmark for its performance, we now perform high-power optical readout using the configuration depicted in Fig. 1b. The 31 μW optical pump is pulsed in unison with the readout pulse using an acousto-optic modulator. Between shots, a pause of 250 μs is inserted to allow the qubit to reset through longitudinal relaxation ($T_1 \approx 60 \mu\text{s}$),

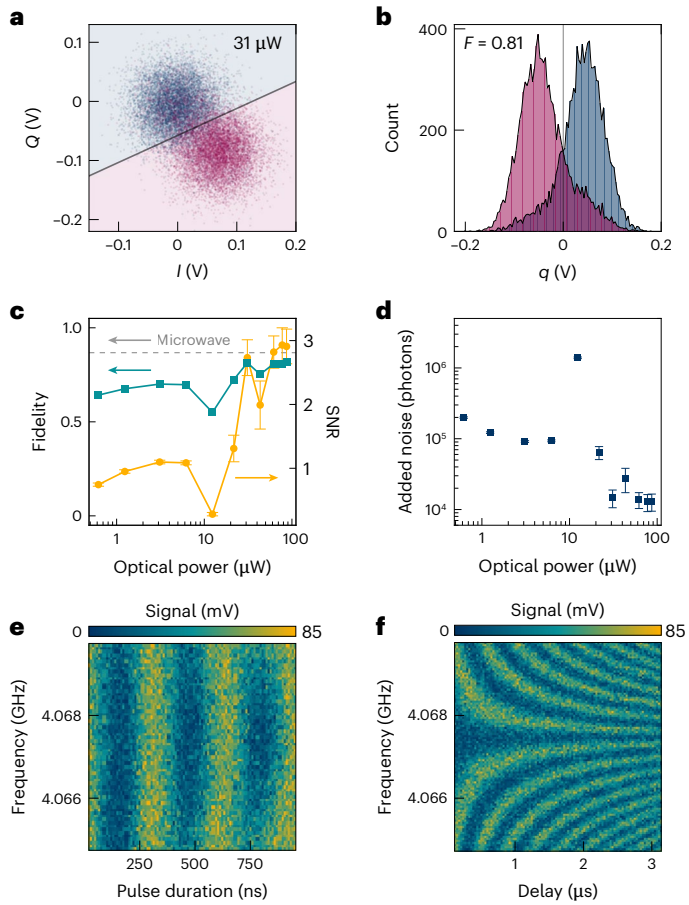


Fig. 3 | Optical qubit readout. **a**, Statistical characterization of 10,000 single-shot optical readout measurements using 31 μW of optical pump power. **b**, The data from **a** binned by the distance to a linear decision boundary q . **c**, Optical readout fidelity (left axis) and SNR (right axis) as a function of optical pump power. The dashed line highlights the microwave readout fidelity. The dip at 12.4 μW is attributed to a transition in the optically dependent phase response of the microwave resonator of the transducer (Supplementary Section II). **d**, The input-referred added noise as a function of optical pump power in units of photons. All error bars are s.d. **e,f**, A Rabi chevron pattern (**e**) and Ramsey fringes (**f**) measured using optical readout.

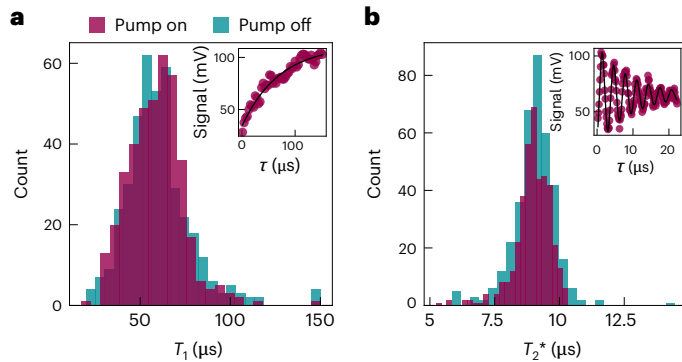


Fig. 4 | Absence of pump-induced decoherence. **a**, Statistical distributions of 401 T_1 measurements, comparing the decay times with a 3.1 μW optical pump on (purple) and off (cyan) yielding $60.2 \pm 3.6 \mu\text{s}$ versus $58.9 \pm 3.0 \mu\text{s}$. **b**, A comparison of the statistical distributions of 401 T_2^* measurements with the pump on (purple) and off (cyan) yielding $8.97 \pm 0.17 \mu\text{s}$, versus $9.03 \pm 0.14 \mu\text{s}$. The insets in both panels show respective example curves with the optical pump on.

yielding an average power delivered into the cryostat of 1.7 μW at a 5.3% duty cycle. Using the same procedure as for microwave-only readout, we recover a single-shot optical readout fidelity of around 81% after 10,000 measurements (Fig. 3a,b). Figure 3c shows the readout fidelity and SNR, determined from bimodal Gaussian fits, as a function of optical power. We find that, at low-to-moderate optical powers, the experimentally determined fidelity is close to the theoretically maximum achievable value of 70% for an SNR near unity³⁶. At high optical power, the experimental fidelity of 82% falls short of the theoretical maximum of ~93% for an SNR of -3, suggesting an important contribution of uncontrolled switching events. However, the SNR of the optical readout is lower than that of the microwave-only readout by a factor of ~25 owing to a considerably larger added noise value. Figure 3d shows the added noise as a function of optical power, which decreases from -2×10^5 photons to -1×10^4 photons as the optical power is increased from 0.6 μW to 87 μW . We estimate the heterodyne shot noise contribution to be around 2×10^3 photons, which dominates over thermal noise. However, an additional noise source, possibly shot noise introduced by the optical pump, ultimately limits the single-shot readout fidelity. We refer the reader to Supplementary Section III for a detailed breakdown and analysis of the added noise. Nevertheless, we find that our optical readout technique is quite suitable for canonical qubit characterizations such as Rabi spectroscopy and Ramsey interferometry (Fig. 3e,f).

At large optical pump powers, thermal microwave photons emitted from the transducer may cause qubit decoherence. In a recent work, it was shown that transverse qubit decay can be mitigated through implementation of sufficient isolation from a microwave transducer pump²¹. We therefore proceed to characterize qubit longitudinal and transverse decay times by measuring T_1 and T_2^* with 60 dB of isolation between the transducer and qubit readout resonator. The transducer microwave reflection output is sent to a HEMT microwave amplifier at 4 K and used to determine the T_1 and T_2^* decay times using microwave-only readout, comparing scenarios with an optical transducer pump of 3.1 μW continuously on or off. To obtain a robust estimation, we perform 401 measurements for each scenario. Figure 4a shows the distribution of the extracted T_1 times, with the inset illustrating an example curve and corresponding fit. We find no statistical difference in the mean T_1 with the pump off ($60.2 \pm 3.6 \mu\text{s}$) and the pump on ($58.9 \pm 3.0 \mu\text{s}$). Likewise, in Fig. 4b no statistical difference in the mean T_2^* with pump off ($9.03 \pm 0.14 \mu\text{s}$) and pump on ($8.97 \pm 0.17 \mu\text{s}$) can be observed. With reduced isolation between the qubit and the transducer, emitted microwaves from the transducer do have an impact on the qubit coherence and the variance of T_1 and T_2^* (Supplementary

Section IV), which has also been a major limitation for quantum transduction when placing the qubit on the same chip as the transducer¹¹. However, 60 dB of isolation is sufficient to prevent backaction of the transducer on the qubit, highlighting the importance of a modular approach of qubit and transduction technology for practical scaling of quantum computers.

Optical readout through a transducer and a fibre opens up new possibilities for configuration of the readout chain in fridges. In particular, a HEMT amplifier dissipates typically close to 10 mW of power, which constitutes a substantial thermal load on the 4 K plate. The microwave-to-optics transducer dissipates a maximum power of 31 μW , which is further decreased by the readout duty cycle. The transducer could also be placed on the still of the dilution refrigerator, dissipating only a small fraction of the available cooling power³⁷ and completely removing the cabling and amplifier heat loads from higher stages. One possible extension is to use transducers as a source for microwave control signals³⁸ or for the generation as well as detection of readout signals, as demonstrated in recent work²². Decreasing the isolation to admit an excitation signal may decrease the T_2^* of the qubit while the transducer optical pump is on, but the pulsed approach used here would protect the qubit during operations. A space-efficient solution could be to include on-chip Purcell filters^{39–41} and isolators⁴² and to use small-form-factor coaxial flex-cabling between stages and modules^{43,44}.

Added noise in our current setup prevents us from fully matching the microwave-only readout performance. Extra local oscillator photons causing this noise can, however, be removed through optical filtering outside the dilution refrigerator, reducing the added noise by -7.7 dB and enabling the full potential of our optical qubit readout scheme. In addition, we anticipate that better frequency matching between the transduction frequency and the qubit readout resonator as well as improvement in transducer cooperativity matching will improve the transduction efficiency by 3 dB and 6 dB, respectively, and, accordingly, the added noise by 10 dB. Finally, adding in a quantum-limited amplifier, such as a travelling wave parametric amplifier or Josephson parametric amplifier, could further reduce the noise by at least 20 dB (ref. 37). In the future, alternative transducer geometries such as optically overcoupled two-dimensional photonic crystals could reduce the optical pump power and the thermal noise such that isolation from the qubit is no longer required^{45,46}. These improvements will result in an optical readout system with close to quantum-limited performance that could perform non-demolition qubit readout with high fidelity and shorter pulse lengths while at the same time substantially reducing the heat load on the dilution refrigerator compared with all-microwave readout approaches.

In summary, we have demonstrated high-power optical qubit readout using a scalable integrated piezo-optomechanical transducer with a single-shot fidelity of 81%. These transducers could be arrayed together to enable the readout of thousands of superconducting qubits in a cryogenic environment, expanding the size of quantum processors in a single dilution refrigerator.

Online content

Any methods, additional references, Nature Portfolio reporting summaries, source data, extended data, supplementary information, acknowledgements, peer review information; details of author contributions and competing interests; and statements of data and code availability are available at <https://doi.org/10.1038/s41567-024-02742-3>.

References

1. 40 years of quantum computing. *Nat. Rev. Phys.* <https://doi.org/10.1038/s42254-021-00410-6> (2022).
2. Arute, F. et al. Quantum supremacy using a programmable superconducting processor. *Nature* **574**, 505–510 (2019).
3. Zhong, H.-S. et al. Quantum computational advantage using photons. *Science* **370**, 1460 (2020).

4. Brooks, M. What's next for quantum computing. *MIT Technology Review* <https://www.technologyreview.com/2023/01/06/1066317/whats-next-for-quantum-computing> (2023).
5. Kjaergaard, M. et al. Superconducting qubits: current state of play. *Annu. Rev. Condens. Matter Phys.* **11**, 369–395 (2020).
6. Chow, J., Dial, O. & Gambetta, J. IBM quantum breaks the 100-qubit processor barrier. *IBM Research Blog* <https://research.ibm.com/blog/127-qubit-quantum-processor-eagle> (2021).
7. The quantum computing learning journey. *Google Quantum AI* <https://quantumai.google/learn/map> (2023).
8. Rigetti investor presentation. *Rigetti Computing* <https://investors.rigetti.com/static-files/fbac3801-223f-4f0f-a207-47d25084a1d7> (2023).
9. We made 1,000 qubits for quantum computing possible. *Bluefors* <https://bluefors.com/blog/we-made-1-000-qubits-for-quantum-computing-possible/> (2023).
10. Preskill, J. Quantum computing in the NISQ era and beyond. *Quantum* **2**, 79 (2018).
11. Mirhosseini, M., Sipahigil, A., Kalaei, M. & Painter, O. Superconducting qubit to optical photon transduction. *Nature* **588**, 599–603 (2020).
12. Han, X. et al. Cavity piezo-mechanics for superconducting–nanophotonic quantum interface. *Nat. Commun.* **11**, 3237 (2020).
13. Han, X., Fu, W., Zou, C.-L., Jiang, L. & Tang, H. X. Microwave-optical quantum frequency conversion. *Optica* **8**, 1050 (2021).
14. Wang, C. et al. High-efficiency microwave-optical quantum transduction based on a cavity electro-optic superconducting system with long coherence time. *npj Quantum Inf.* **8**, 149 (2022).
15. Meesala, S. et al. Non-classical microwave-optical photon pair generation with a chip-scale transducer. *Nat. Phys.* **20**, 871–877 (2024).
16. Jiang, W. et al. Optically heralded microwave photon addition. *Nat. Phys.* **19**, 1423–1428 (2023).
17. Lecocq, F. et al. Control and readout of a superconducting qubit using a photonic link. *Nature* **591**, 575–579 (2021).
18. Pobell, F. *Matter and Methods at Low Temperatures* 3rd edn (Springer, 2007); <https://doi.org/10.1007/978-3-540-46360-3>
19. MacDonald, A. et al. Optical microscope and tapered fiber coupling apparatus for a dilution refrigerator. *Rev. Sci. Instrum.* **86**, 013107 (2015).
20. Corcoran, B. et al. Ultra-dense optical data transmission over standard fibre with a single chip source. *Nat. Commun.* **11**, 2568 (2020).
21. Delaney, R. et al. Superconducting-qubit readout via low-backaction electro-optic transduction. *Nature* **606**, 489–493 (2022).
22. Arnold, G. et al. All-optical single-shot readout of a superconducting qubit. Preprint at <https://doi.org/10.48550/arXiv.2310.16817> (2023).
23. Weaver, M. J. et al. An integrated microwave-to-optics interface for scalable quantum computing. *Nat. Nanotechnol.* **19**, 166–172 (2024).
24. Rigetti quantum foundry services. *Rigetti Computing* <https://www.rigetti.com/rigetti-quantum-foundry-services>. Accessed 19 Jan 2024.
25. Andrews, R. W. et al. Bidirectional and efficient conversion between microwave and optical light. *Nat. Phys.* **10**, 321–326 (2014).
26. Google Quantum AI. Suppressing quantum errors by scaling a surface code logical qubit. *Nature* **614**, 676–681 (2023).
27. Aspelmeyer, M., Kippenberg, T. J. & Marquardt, F. Cavity optomechanics. *Rev. Mod. Phys.* **86**, 1391 (2014).
28. Xu, M., Han, X., Fu, W., Zou, C.-L. & Tang, H. X. Frequency-tunable high-Q superconducting resonators via wireless control of nonlinear kinetic inductance. *Appl. Phys. Lett.* **114**, 192601 (2019).
29. Reed, M. et al. High-fidelity readout in circuit quantum electrodynamics using the Jaynes–Cummings nonlinearity. *Phys. Rev. Lett.* **105**, 173601 (2010).
30. Boissonneault, M., Gambetta, J. & Blais, A. Improved superconducting qubit readout by qubit-induced nonlinearities. *Phys. Rev. Lett.* **105**, 100504 (2010).
31. Bishop, L. S., Ginossar, E. & Girvin, S. Response of the strongly driven jaynes-cummings oscillator. *Phys. Rev. Lett.* **105**, 100505 (2010).
32. Qubit readout module (QRM) datasheet. Qblox <https://docs.qblox.com/en/main/cluster/qrm.html> (2024).
33. Wenner, J. et al. Excitation of superconducting qubits from hot nonequilibrium quasiparticles. *Phys. Rev. Lett.* **110**, 150502 (2013).
34. Geerlings, K. et al. Demonstrating a driven reset protocol for a superconducting qubit. *Phys. Rev. Lett.* **110**, 120501 (2013).
35. Jin, X. et al. Thermal and residual excited-state population in a 3D transmon qubit. *Phys. Rev. Lett.* **114**, 240501 (2015).
36. Chen, L. et al. Transmon qubit readout fidelity at the threshold for quantum error correction without a quantum-limited amplifier. *npj Quantum Inf.* **9**, 26 (2023).
37. Krinner, S. et al. Engineering cryogenic setups for 100-qubit scale superconducting circuit systems. *EPJ Quant. Technol.* **6**, 2 (2019).
38. Warner, H. et al. Coherent control of a superconducting qubit using light. Preprint at <https://doi.org/10.48550/arXiv.2310.16155> (2023).
39. Reed, M. D. et al. Fast reset and suppressing spontaneous emission of a superconducting qubit. *Appl. Phys. Lett.* **96**, 203110 (2010).
40. Jeffrey, E. et al. Fast accurate state measurement with superconducting qubits. *Phys. Rev. Lett.* **112**, 190504 (2014).
41. Sete, E. A., Martinis, J. M. & Korotkov, A. N. Quantum theory of a bandpass purcell filter for qubit readout. *Phys. Rev. A* **92**, 012325 (2015).
42. Chapman, B. J. et al. Widely tunable on-chip microwave circulator for superconducting quantum circuits. *Phys. Rev. X* **7**, 041043 (2017).
43. Smith, J. P., Mazin, B. A., Boaventura, A., Thompson, K. J. & Daa, M. Improved flexible coaxial ribbon cable for high-density superconducting arrays. *IEEE Trans. Appl. Superconduct.* <https://doi.org/10.1109/TASC.2024.3350516> (2024).
44. Monarkha, V. Y. et al. Equivalence of flexible stripline and coaxial cables for superconducting qubit control and readout pulses. *Appl. Phys. Lett.* **124**, 224001 (2024).
45. Sonar, S. et al. High-efficiency low-noise optomechanical crystal photon–phonon transducers. Preprint at <https://doi.org/10.48550/arXiv.2406.15701> (2024).
46. Chen, L. et al. Bandwidth-tunable telecom single photons enabled by low-noise optomechanical transduction. Preprint at <https://doi.org/10.48550/arXiv.2410.10947> (2024).

Publisher's note Springer Nature remains neutral with regard to jurisdictional claims in published maps and institutional affiliations.

Springer Nature or its licensor (e.g. a society or other partner) holds exclusive rights to this article under a publishing agreement with the author(s) or other rightsholder(s); author self-archiving of the accepted manuscript version of this article is solely governed by the terms of such publishing agreement and applicable law.

© The Author(s), under exclusive licence to Springer Nature Limited 2025

Data availability

Source data for the figures are available via Zenodo at <https://doi.org/10.5281/zenodo.1429325>.

Acknowledgements

We acknowledge assistance from E. He and the hospitality of the Department of Quantum Nanoscience at Delft University of Technology, as well as the Kavli Nanolab Delft. QphoX also thanks the European Innovation Council (EIC Accelerator QModem 190109269) for financial support. Qblox acknowledges support from the European Commission under grant agreement 969201.

Author contributions

T.C.v.T., M.J.W., M.Ž., F.H., R.S. and S.G. designed the experiment. T.C.v.T., M.J.W., P.D., M.Ž., A.C.B., C.F. and E.C. collected and analysed the data. F.B., P.D., M.L., K.L.S. and R.S. designed and fabricated the transducer device. F.K.d.V., C.C.B. and J.C.v.O. designed electronic hardware for qubit operation and data acquisition. E.L., M.F., Y.M. and J.Y.M. provided qubit and mounting hardware, as well as experimental support. T.C.v.T., M.J.W., R.S. and S.G. wrote the paper with input from all authors.

Competing interests

The authors declare the following competing interests: T.C.v.T., M.J.W., F.B., P.D., M.L., K.L.S., M.Ž., F.H., A.C.B., C.F., E.C., R.S. and S.G. are or have been employed by QphoX B.V. and are, have been or may in the future be participants in incentive stock plans at QphoX B.V. F.K.d.V., C.C.B. and J.C.v.O. declare a financial interest in Qblox B.V. J.Y.M., M.F., E.L. and Y.M. are or have been employed by Rigetti & Co, LLC. J.Y.M., M.F., E.L. and Y.M. are, have been or may in the future be participants in incentive stock plans at Rigetti & Co, LLC.

Additional information

Supplementary information The online version contains supplementary material available at <https://doi.org/10.1038/s41567-024-02742-3>.

Correspondence and requests for materials should be addressed to R. Stockill or S. Gröblacher.

Peer review information *Nature Physics* thanks the anonymous reviewers for their contribution to the peer review of this work.

Reprints and permissions information is available at www.nature.com/reprints.